CLIMATIC CHARACTERISTICS OF EARTH–ATMOSPHERE OUTGOING LONGWAVE RADIATION OVER CHINA *

Weng Duming (翁笃鸣) * *

Nanjing Institute of Meteorology, Nanjing 210044

Received March 10, 1994; revised December 21, 1994

ABSTRACT

ERBE and ISCCP data are used to investigate the cloud forcing and latitude and atmospheric temperature effects on outgoing longwave radiation (OLR) in the earth–atmosphere system, and the similarity of OLR field to 500 hPa and surface effective radiation fields. Also, discussion is taken up of the OLR distribution on a nationwide basis, indicating that the winter (summer) OLR pattern is roughly a zonal type (asymmetrical saddle) with the annual pattern analogous to the January one. In the end the yearly OLR variation features are addressed on a regional basis.

Key words: China, outgoing longwave radiation (OLR), climatic characteristics

The study of earth–atmosphere OLR distribution and variation is of much importance to the understanding of regional climatic formation and change and thus one of the subjects so vital in modern climatology as to draw widespread attention (e. g. Kondratyev et al. 1988). Such research has just been begun in China with only a small part concerning OLR climatic features with applications in the Qinghai–Xizang Plateau (QXP) and some stations (Kang and Wu 1990; Jiang et al. 1991; Chen and Xie 1987) so that no complete analysis exists of the nationwide OLR in a climatological context.

The present work is an attempt to make further study in this scope in order to provide a basis for overall examination of the OLR and thermal–source features in this country. The data used come from 1985—1988 ERBE (Earth Radiation Balance Experiment) clear–sky and mean OLR (Barkstrom 1984) and the average total cloudiness of synchronous ISCCP (International Satellite Cloud–Climate Programme, see Rossow and Schiffer 1991) with the domain covering China mainland and its surroundings, having a grid spacing of 2. $5^\circ \times 2.5^\circ$ latitude / longitude. It is noted that the present work is in part based on the calculations on ground and atmospheric effective radiation in a previous study of the author.

I. CORRELATIVITY OF OLR AFFECTING FACTORS AND OTHER RADIATION ELEMENTS

1. *Cloud Forcing on OLR*

Clear–sky OLR is dependent largely on longwave radiation from the underlying surface and atmosphere. Under a cloudy sky, however, OLR is weakened because of cloud radiative attributes and cloud–top temperature markedly lower than that at the same level of the air,

* The work is sponsored by the National Natural Sciences Foundation of China.

* * This study involves part of the work done by Li Ju, graduate of 1989 class of the institute.

leading to the fact that difference represents the forcing of cloud on OLR as one of its important climatic features.

Figure 1 depicts the relation of monthly cloud forcing on OLR (ΔF_∞) to mean global cloud amount for 10 stations, including Beijing, Haikou, Ganzhou, Shanghai, Nanning, Wuhan, Kunming, Lhasa, Harbin and Urumqi (the same below). The tendency of the scattering distribution on the plot shows that the forcing is enhanced with the increase in total cloudiness, which can be roughly represented by a monotonous curve. And the result from simple linear fitting is given by the broken line.

To make further analysis of cloud effect, a statistical analysis is conducted of the correlation coefficients between global cloudiness and OLR on a monthly basis in the mainland and its surroundings (21—57°N, 61—150°E), as shown in Table 1. Clearly, correlation for the large-scale area exists in the warm months (April—October) with the June and July negative correlation being strongest in contrast to the cold season marked even by a reversed sign. The cause may presumably be associated with the seasonal change in the underlying surface thermal states and atmospheric temperature distribution. In contrast, warm-season temperature is relatively homogeneous, making for the intense forcing upon OLR, especially in summer months. To the contrary, the winter temperature difference becomes vast from region to region, thus masking the cloud-OLR correlativity.

Table 1. Total Cloudiness-OLR Correlations over China and Its Surroundings ($n = 170$)

Month	Jan.	Feb.	Mar.	Apr.	May	Jun.	Jul.	Aug.	Sep.	Oct.	Nov.	Dec.
r_n, F_∞	0.111*	0.055*	−0.133*	−0.479	−0.685	−0.809	−0.794	−0.619	−0.729	−0.413	−0.187*	0.064*

Note: The asterisked figures denote that the calculations have not passed t-test at 0.01 confidence level (the same below).

Table 2. Mean Total Cloudiness-OLR Correlation Statistics with the Regression Errors on a Regional Basis

Region	Sample size	January			July			Annual-mean		
		r	δF_∞	$\frac{\Delta F_\infty}{F_\infty}$	r	δF_∞	$\frac{\Delta F_\infty}{F_\infty}$	r	δF_∞	$\frac{\Delta F_\infty}{F_\infty}$
N, NW, NE China (N of 37.5°N)	87	−0.650	8.7	0.064	−0.893	4.5	0.019	−0.648	4.4	0.032
QXP (S of 37.5°N, W of 105° E)	42	−0.083*	18.3	0.093	−0.829	9.5	0.043	−0.246*	13.7	0.064
E China (S of 37.5°N, W of 105° E)	41	−0.286*	21.0	0.090	−0.711	9.8	0.043	0.030*	9.8	0.042
Nationwide mean	170	0.199*	24.4	0.119	−0.898	11.3	0.048	−0.084*	11.8	0.055

Note: For the areas whose correlation coefficients have failed to pass t-test at 0. 01 confidence level, δF_∞ denotes the root mean square deviation of OLR (the same below).

Table 2 presents the total cloudiness-OLR correlation coefficients and relative regression errors for January, July and annual means with the total results in agreement with those of Table 1. The regional calculations are employed to discriminate the discrepancy in the related

sectors and to improve retrieval effectiveness. The July (typical of summer) correlation is higher for all the regions in Table 2, and inter-regional correlation between the January and annual mean cloudiness-OLR is quite low, failing to pass t-test at 0. 01 credibility except N, NW and NE China.

Table 3. Planetary Albedo-OLR Correlations and the Regression Errors

Region	Sample size	January			July			Annual mean		
		r	δF_∞	$\frac{\Delta F_\alpha}{F_\infty}$	r	δF_∞	$\frac{\Delta F_\alpha}{F_\infty}$	r	δF_∞	$\frac{\Delta F_\alpha}{F_\infty}$
N, NW, NE China (N of 37.5°N)	87	−0.704	8.2	0.043	−0.944	3.3	0.014	−0.687	6.8	0.031
QXP (S of 37.5°N, W of 105° E)	42	−0.828	10.3	0.053	−0.814	10.0	0.045	−0.782	8.5	0.040
E China (S of 37.5°N, W of 105° E)	41	−0.197*	21.0	0.090	−0.820	8.0	0.035	0.012*	9.8	0.042
Nationwide mean	170	−0.369	22.7	0.111	−0.866	12.9	0.055	−0.105*	17.4	0.079

Planetary-scale reflectivity is well correlated with OLR condition, implying an association between them under the action of the same factor—total cloudiness, with the correlation and regression statistics summarized in Table 3. Comparison of Tables 3 and 2 indicates that the planetary albedo-OLR correlations and regression are somewhat better than the cloudiness-OLR relation, particularly in the Qinghai-Xizang Plateau.

2. *Effect on OLR of Latitude and Atmospheric Temperature*

The OLR impact of latitude is exerted mainly through the surface thermal regime of the latitudes with the latitude circle averaged OLR (W / m^2) over 105—115°E in the Northern Hemisphere given in Table 4 to show the change at an increment of 5° latitude.

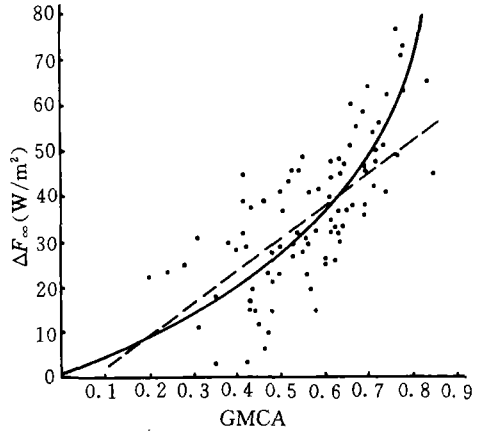

Fig. 1. Change in cloud forcing on OLR with global mean cloud amount (GMCA).

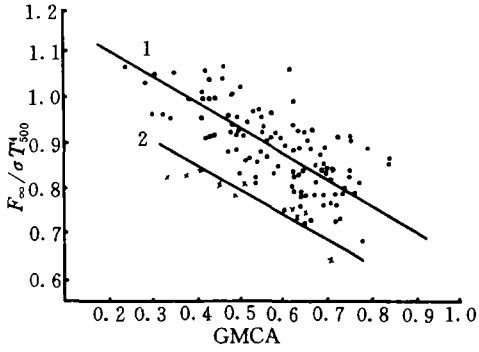

Fig. 2. Correlation between $F_\infty / \sigma T_{500}^4$ and global mean cloud amount (GMCA) for the 10 stations with the inclusion of Beijing, (a) for Beijiing and the other 9 stations; (b) for Lhasa.

Table 4. Impact of Latitude on OLR

		Latitude (°N)					
		25	30	35	40	45	50
Jan.	F_∞	249.4	222.4	212.1	201.9	186.2	178.5
	S_0	281.1	247.6	213.0	177.5	154.6	106.6
July	F_∞	233.5	234.0	243.4	249.6	246.2	232.0
	S_0	468.1	475.8	480.8	483.1	483.0	481.0
Annual mean	F_∞	241.8	231.0	225.9	225.0	218.2	205.4
	S_0	388.1	388.6	346.5	321.8	249.7	265.3

The related astronomical radiation S_0 is also given in the table for comparison. It is seen that the trend of the latitudinal change of OLR is in rough agreement with that of S_0, suggesting the major influence of latitude as a permanent factor.

The underlying surface and atmospheric temperature serve as principal factors controlling the OLR regime. It is reported that OLR is parameterized simply with the surface or atmospheric temperature (Kondratyev et al. 1988), which leads only to rough approximation, however. It seems more reasonable to couple temperature with mean cloudiness to express OLR in an approximate fashion, viz.:

$$F_\infty \approx \sigma T_{500}^4 f(n),$$

where T_{500} is the 500 hPa temperature, σ the Stefan–Boltzmann constant, n the total cloudiness and $f(n)$ determined empirically. The applicability and rationality of the expression for F can be demonstrated by verification against the measurements. For this reason, prepared is a scatter plot of $F_\infty / \sigma T_{500}^4$ and n for 10 stations mentioned earlier (Fig. 2), where the scattering dots distributed in a reasonable pattern, thereby allowing to distinguish the Lhasa regime from that of the others, to which the fitting of a respective regression expression is performed with the parameters and relative regression errors given in Table 4. All these visual devices demonstrate stronger correlation between $F_\infty / \sigma T_{500}^4$ and the total cloudiness and around 7% for the errors; the slope is similar for both the equations and the difference in intercept reveals effects of altitude above sea level.

Table 5. Parameters of the Regression Equation for $F_\infty / \sigma T_{500}^4$ and the Total Cloudiness with the Relative Regression Errors (*RRE*)

Station	r	a	b	*RRE*
Beijing and other 9 stations	−0.709	1.161	−0.478	0.071
Lhasa	−0.814	1.020	−0.483	0.059

3. *Correlativity between OLR and Effective Radiation from Atmosphere and Surface*

Calculated are similarity coefficients between patterns of OLR and effective radiation (ER) from the atmosphere and ground (Table 6), with the ER values for 500 hPa level and surface coming directly from Sun and Weng (1986) and Weng and Ren (1994). Table 6 illustrates stronger similarity between patterns of OLR and the ER F_{500} except OLR similarity to F_{500} on an annual basis over the Qinghai–Xizang Plateau, the latter being homogeneous in pattern, leading to the root mean square deviation of 2.0 W / m^2 only.

One can see poor similarity between patterns of OLR and surface ER except Region 1. This

problem has been addressed in foreign literatures (Kondratyev et al. 1988) and may be related to the differential influence of cloud nature on OLR and surface ER. Generally, mid to high and vertical-development clouds with tops reaching high levels have maximum effect whilst clouds with lower base exert marked impact on surface ER, leading to reduced correlation between OLR and ground ER so that the similarity coefficients for the regions or seasons in Table 6 have opposite sign. Further, calculations of the regression errors on the nationwide and regional bases suggest that the retrieval from OLR to 500 hPa ER yields satisfactory results in contrast to the performance for surface ER which results in errors of $>15\%$.

Table 6. Similarity Coefficients between Patterns of OLR and Effective Radiation from 500 hPa Level and Ground on a Regional Basis

	$r_{F_\infty \cdot F_{500}}$				$r_{F_\infty \cdot F}$			
	Region 1	Region 2	Region 3	Nationwide	Region 1	Region 2	Region 3	Nationwide
January	0.553	0.775	0.969	0.740	0.649	0.245*	−0.351*	−0.079*
July	0.726	0.994	0.703	0.871	0.735	0.902	0.470*	0.382*
Annual	0.789	−0.238*	0.905	0.481	0.584	−0.363*	−0.690*	−0.512

Note: (1) Region 1 for N, NW and NE China; Region 2 for the Qinghai–Xizang Plateau; Region 3 for E China. (2) The critical similarity coefficients differ because of the different degrees of freedom.

II. SPACE AND TIME PATTERNS OF OLR

1. *OLR Pattern on a Nationwide Basis*

The OLR nationwide distribution is featured by strong monsoon climate in association with the atmospheric circulation and geography.

Winter (January) OLR on a nationwide basis is in accord with temperature distribution under the action of severe winter monsoon, with higher (lower) values in the south (north) and particularly east of 105°E, as shown in Fig. 3. And over West China under the effect of topography and especially under the influence of cloud and the underlying surface there arises a pattern of high-value areas alternated with low-value sectors with the high center in the Tarim Basin, maximizing at >200 W / m^2, a result from scattered or cloud-free sky and the terrain of higher surface temperature; in the Qinghai–Xizang Plateau, effects of enhanced cloudiness and snow cover are responsible for a relatively low-value sector, centered (<180 W / m^2) on the windward side of the western highland, in relation to the seasonal cloud band and high-planetary albedo zone. Calculations indicate that the January OLR and mean temperature have the similarity coefficient reaching as much as 0.946, and in comparison to the patterns of summer and yearly mean OLR, the winter isopleths are very close with maximum gradients in the eastern part of the plateau and its neighboring area.

In contrast, the summer (July) OLR field assumes an asymmetric saddle form (Fig. 4). The principal high-value area (>270 W / m^2) is in the arid climate region of West China centered at the Tarim Basin and related to the aridity, scattered or cloud-free sky and severe hotness under the control of the continental thermal low. Under the control of the subtropical high the high-value belt extends eastward into the lower reach of the Huanghe River and North China Plains, with its SE segment close to the high-value belt of OLR stretching from the western Pacific into the area south of the lower reach of the Changjiang River and coastal regions whilst

the principal low band covers the whole SW China and the southern and SE parts of the Plateau and the western part of South China, implying the intense effects of SW monsoon. In this vast area, however, severe convective cloud development will give rise to sharply reduced OLR with < 200 W / m^2 over the Yarlung Zangbo River basin and the Hengduan Mountains east of the Plateau; the low segment is not obvious over the SE portion of NE China plain on account

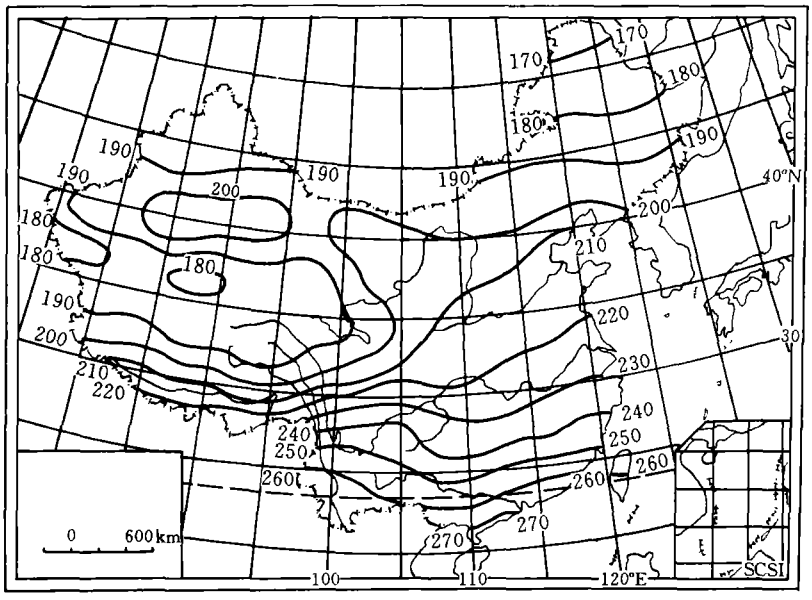

Fig. 3. January OLR pattern on a nationwide basis (W / m^2).

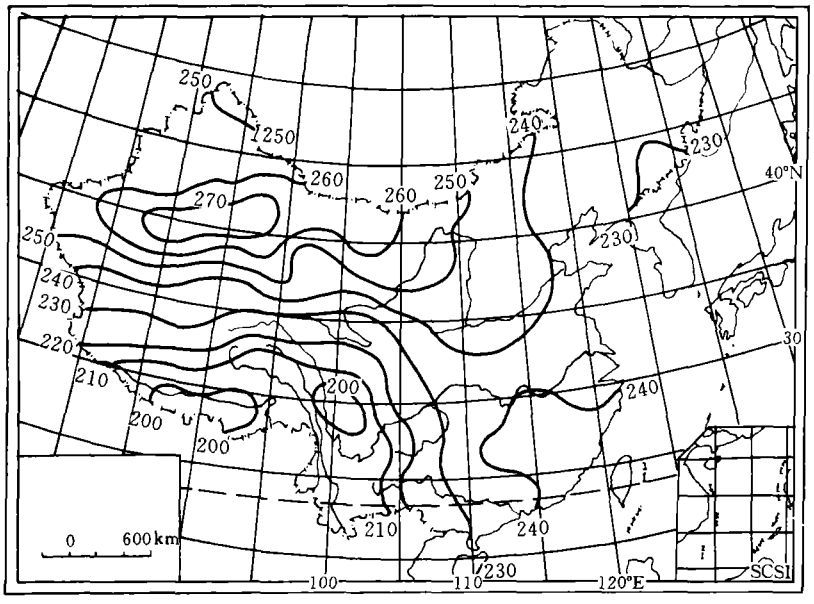

Fig. 4. July OLR pattern over China (W / m^2).

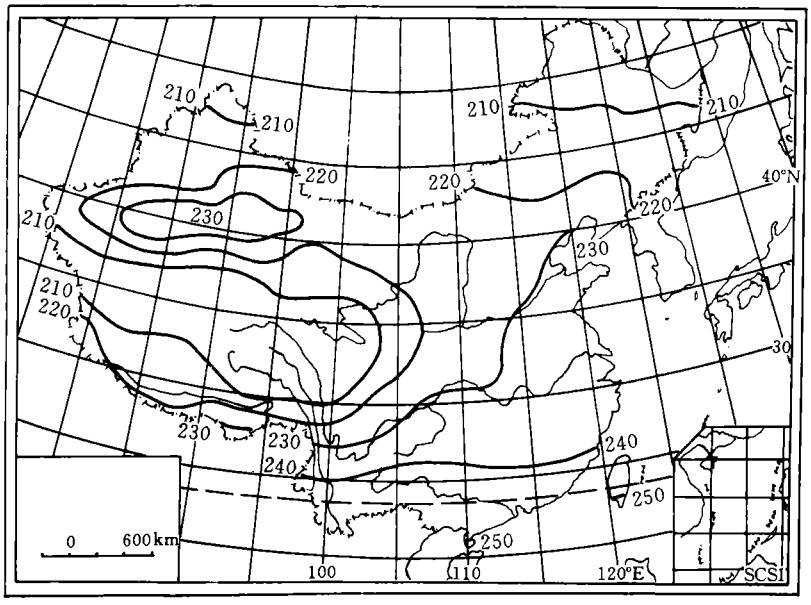

Fig. 5. Nationwide annual mean OLR pattern (W / m^2).

of the association with SE monsoon, on which, in reality, the summer OLR magnitude depends over the whole NE China Plains and part of North China and Inner Mongolia.

On the whole, the distribution of summer OLR is in good correspondence to those of the total cloudiness and planetary albedo, leading to the similarity coefficients as high as −0.898 and −0.866, respectively, suggesting that cloud impact is decisive with a more homogeneous temperature pattern over the land, which should be regarded as a distinctive feature of OLR influence of the monsoon climate. Further, found out statistically is July OLR / rainfall similarity coefficient of 0.629 compared to 0.516 for January, implying enhanced convective precipitation in July.

The annual OLR pattern is more similar to the winter situation (Fig. 5) with a coefficient of 0.846, indicating the important role of such permanent factors as latitude and terrain. And the isolines are relatively sparser with small change in magnitude, i.e., < 50 W / m^2 for the country as a whole.

2. *OLR Annual Course*

As another important climatic feature, the regional OLR cycle shows the role of seasonality and cloudiness, which is given in Fig. 6, illustrating the OLR yearly course for 8 representive regions of the land, based mainly on climatic condition and physical geography; each of regions is represented by the average over 4 gridpoints in it. This will diminish the influence of random factors, to some extent.

One can see that curves 1 and 5 are V−shaped, showing the leading effects of cloudiness at low latitudes; curve 6 in zigzag form displays higher cloudiness with a small change in value ($\sim$ 20 W / m^2); curves 2 and 3 are analogous to each other in that the maximum (minimum) arises in August (Febuary—March), with a minor minimum in June over that region due to the Mei−yu rainfall; curves 4 and 7 are similar in form, exhibiting a valley in July—August (the

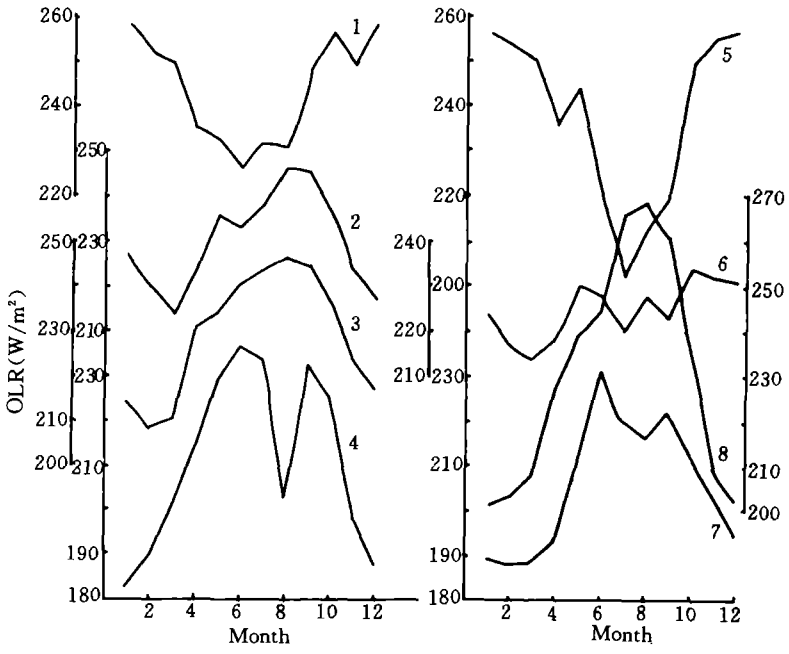

Fig. 6. Annual OLR course on a regional basis. 1. S China coastal area (22.5—25. 0°N, 105—115°E); 2. lower reach of the Changjiang River (27.5—32. 5°N, 115—120°E); 3. N China Plains (35—40°N, 112.5—117.5°E); 4. NE China Plains (45—50°N, 122.5—127.5°E); 5. SW Yunnan (22.5—27.5°N, 97.5—102.5°E); 6. Sichuan Basin (30—35°N, 102.5—107.5°E); 7. QXP (27.5—32.5°N, 85—90°E); 8. NW China arid area (40—45°N, 90—95°E).

former being influenced by SE monsoon and the latter by Indian monsoon), with the maximum appearing in June ahead of the rainy season or in its early phase; curve 8 indicates a normal type of extratropical OLR except that the appearing time (months) of maximum and minimum lays behind that of surface radiation elements, implying the impact of atmospheric temperature change features, a phenomenon that is also clearly shown in the appearing period of yearly minimum for the other regions under study.

III. CONCLUDING REMARKS

From the above analysis we arrive at the following:

(1) The OLR change depends on latitude, season, cloud, the underlying surface and atmospheric temperature, the first two determining its basic trend and the others, especially cloud effect, causing its deviation, with the cloud forcing enhanced with cloudiness.

(2) Strong OLR–cloudiness correlation occurs in warm season (April—October) as opposed to that in other months, so does the planetary albedo–OLR relation, an association between the two types under the action of the same factor—cloud.

(3) The empirical expression $F=T_{500}(a+bn)$ for the derived OLR in relation to 500 hPa temperature and the total cloudiness has shown higher fitting results, and the OLR is found to be in good correlation with atmospheric effective radiation and shows a low similarity coefficient to surface effective radiation, a fact produced by degrees of cloud influence on

radiation.

(4) On a nationwide basis, the zonal pattern is predominant in winter but with a high–value center and a low–value center in the Tarim Basin and northern Qinghai–Xizang Plateau, respectively. In contrast, the summer pattern is in an asymmetric saddle form, the chief high– and low–value regions appearing in arid NW China and SW China including SE Qinghai–Xizang Plateau, respectively. Moreover, a high region and a low region are observed to be the south of the lower reach of the Changjiang River and Southeast and Northeast China Plains, respectively. The annual OLR pattern bears resemblance to that of January but with sharply reduced variation in magnitude.

(5) On a regional basis, the annual OLR course, especially the appearing time (months) of maxima and minima, rests strongly upon cloudiness.

REFERENCES

Barkstrom, B. R. (1984), The earth radiation budget experience (ERBE), *Bull. Amer. Meteor. Soc.*, **65:** 1170—1185.

Chen Longxun and Xie An (1987), The relationship between El Nino and 30—60 day oscillation revealed by OLR data, *Collection of Meteorological Papers*, China Meteorological Press, Beijing, pp. 26—35 (in Chinese).

Jiang Shangcheng, Zhu Yafen and Zhu Yuanjing (1991), The China regional climates observed by meteorological satellites, *Acta Meteor. Sin.*, **49:** 512—517 (in Chinese).

Kang Shanfu and Wu Junming (1990), The climatic characteristics of OLR field over the Qinghai–xizang Plateau, *Plateau Meteorology*, **9:** 98—102 (in Chinese).

Kondratyev, K. Y., Dyachenko, L. N. and Kozoderov, V. V. (1988), *Earth Radiation Budget*, Hydrometeor. Press, pp. 81—120 (in Russian).

Rossow, W. B. and Schiffer, R. A. (1991), ISCCP cloud data products, *Bull. Amer. Meteor. Soc.*, **72:** 2—20.

Sun Zhi'an and Weng Duming (1986), Climatological calculation and distribution features of effective radiation in China (Part II), *J. Nanjing Institute of Meteor.*, **9:** 335—347 (in Chinese).

Weng Duming and Ren Xiaobo (1994), Climatological calculation of atmospheric effective radiation over China, *ibid.*, **17:** 332—337 (in Chinese)